arXiv:1409.5428v1 [astro-ph.GA] 18 Sep 2014

Connecting the interstellar magnetic field at the heliosphere to the Loop I superbubble

P C Frisch[1], A Berdyugin[2], H O Funsten[3], A M Magalhaes[4], D J McComas[5], V Piirola[2], N A Schwadron[6], D B Seriacopi[4], and S J Wiktorowicz[7]

[1]Dept of Astronomy and Astrophysics, University of Chicago, Chicago, IL 60637, USA [2]Finnish Centre for Astronomy with ESO, University of Turku, Finland [3]Los Alamos National Laboratory, Los Alamos, NM [4]Inst de Astronomia, Geofisica e Ciencias Atmosfericas, Universidade de Sao Paulo, Brazil [5]Southwest Research Inst, San Antonio, TX and University of Texas, San Antonio, TX [6]Space Science Center, University of New Hampshire, Durham, NH [7]Dept of Astronomy, University of California at Santa Cruz, Santa Cruz, CA

Abstract

The local interstellar magnetic field affects both the heliosphere and the surrounding cluster of interstellar clouds (CLIC). Measurements of linearly polarized starlight provide the only test of the magnetic field threading the CLIC. Polarization measurements of the CLIC magnetic field show multiple local magnetic structures, one of which is aligned with the magnetic field traced by the center of the "ribbon" of energetic neutral atoms discovered by the Interstellar Boundary Explorer (IBEX). Comparisons between the bulk motion of the CLIC through the local standard of rest, the magnetic field direction, the geometric center of Loop I, and the polarized dust bridge extending from the heliosphere toward the North Polar Spur direction all suggest that the CLIC is part of the rim region of the Loop I superbubble.

1 Origin of local interstellar magnetic field

The Sun resides in a region of space with very low interstellar densities [20] that is offset by ~ 400 pc from the density maximum of the Orion spiral arm (also known as the Orion Spur, 9). The interstellar magnetic field (ISMF) in this interarm region is characterized by an ordered magnetic field with a strength 1.4 ± 0.3 μG that is directed toward the local radiant at $\ell \sim 88°$ in the galactic plane [27; 31; 44]. The older clusters of the Scorpius-Centaurus Association (ScoOB2), located ~ 120 pc from the Sun, are also offset from the density maximum of the Orion arm [9].

A superbubble was created by the ScoOB2 stellar winds and supernova during three epochs of star formation over the past 15 Myrs [7; 8; 11; 38]. A classic expanding superbubble will sweep up the ISMF during expansion, expanding asymmetrically in directions parallel to the ISMF for initially uniform gas, and with the compressed magnetic field lines parallel to the rim of the shell in directions perpendicular to the magnetic field [10; 37; 56]. The epochs of star formation in ScoOB2 swept the expanding superbubble into the interarm region through which the heliosphere moves (Fig. 1, [11; 38**?**]). The interstellar signatures of the Loop I superbubble have been analyzed based on tracers of neutral gas, polarized starlight, and radio continuum emission [3; 4; 7; 8; 28; 32–34; 50].

The original superbubble expanded into a giant dust cloud, the remnants of which form the Aquila Rift molecular cloud, and initiated the sequential star formation that produced the upper Scorpius subgroup [7; 8]. Recent stellar evolution in the upper Scorpius subgroup generated the supernova that produced the bright X-ray source associated with the North Polar Spur radio emission. Observations and models of the X-ray plasma and radio shell show that it is a supernova remnant with an age of ~ 2 Myrs that was reheated possibly within the past 100,000 years [35]. Hydrogen column densities and dust opacity jump at ~ 100 pc in the North Polar Spur segment of Loop I ($330° < \ell < 30°$, $0° < b < 40°$, [35; 47]). Cosmic rays generated in the remnant light up the magnetic field compressed in the superbubble shell with synchrotron emission, producing the giant non-thermal radio continuum feature, Loop I,

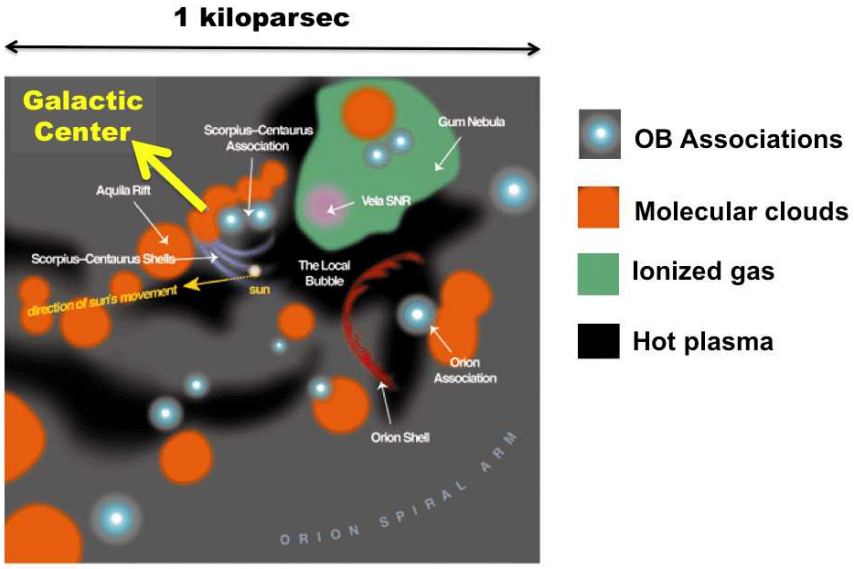

Figure 1: The distribution of molecular clouds (orange) traced by the CO 12 cm line is shown for nearby regions. Stellar associations (bright starry dots) form from these molecular clouds, generating superbubble shells that compress interstellar dust and gas during expansion (gray and red shell-like arcs). The solar motion through the LSR (golden arrow) has carried the Sun through the low density interior of the Local Bubble for the past several million years (figure from [12]).

that dominates the northern hemisphere sky [4]. The magnetic field associated with Loop I dominates starlight polarization in the northern hemisphere [4; 39; 50], and the polarized emission of interstellar dust grains [43].

A coherent picture of the Loop I ISMF can found using three sources of polarized light, starlight polarization, polarized dust emission, and polarized synchrotron emission. Starlight is linearly polarized by asymmetric dust grains that have larger opacities along the axis that is perpendicular to the magnetic field, so that optical polarization vectors are parallel to the magnetic field direction (e.g. [36). The polarized emission of dust grains is parallel to the most optically opaque axis, and therefore perpendicular to the ISMF direction for aligned grains [42; 43]. The polarization of synchrotron emission is aligned with the acceleration vector of electrons and ions propagating along the ISMF, so that it is perpendicular to the ISMF direction for galactic cosmic rays gyrating around the ISMF. The property that the optical polarization vectors are perpendicular to the Loop I synchrotron polarizations (e.g. compare polarization maps in references [39and [4]), and also perpendicular to polarized infrared light from dust associated with Loop I [42; 43], shows that the position angles of polarized starlight trace the magnetic field directions in the global diffuse interstellar medium, and that the linearly polarized starlight has a plane of polarization that is parallel to the magnetic field direction. This property enables the mapping of the local ISMF direction using high-sensitivity polarization measurements, $\leq 0.01\%$ [2; 14; 18; 21; 22]. Fig. 2 shows starlight polarizations plotted over the ISMF direction obtained from measurements of polarized dust emission by Planck [42; 43].

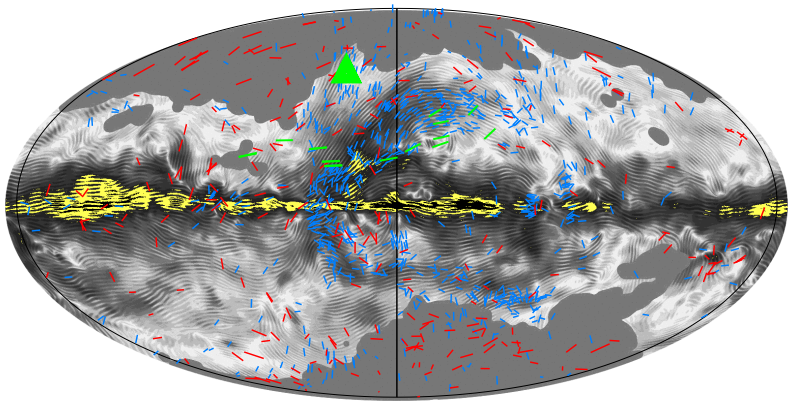

Figure 2: Stellar polarization data are overplotted on the magnetic field direction based on polarized dust emission measured by Planck [Planck Collaboration et al., 2014]. The green triangle shows the direction of the ISMF traced by the center of the IBEX Ribbon arc [Funsten et al., 2013]. A high-latitude dust arc is found in this direction. The blue bars show the polarizations of distant (> 40 pc) stars that trace the maximum of the Loop I intensity. Red bars show polarizations for stars within 40 pc. Green bars show the filament stars that are located toward the inner ridge of the nearby portion of Loop I (Fig. 3). In the northern parts of Loop I and in the first galactic quadrant,, where the ISMF extends to the solar location (Fig. 4), the ISMF direction traced by the optical and infrared polarizations are consistent. Yellow regions appear in sightlines of highest dust emissivity.

Optically polarized starlight reveals the ISMF associated with Loop I [39]. Polarization surveys by Mathewson and Ford [39], Santos et al. [50] and Berdyugin et al. [3] have mapped starlight polarizations that trace the ISMF of Loop I. Dust extinction and polarization strengths jump at 100 ± 20 pc where $\ell < 40°$, and at 280 ± 50 pc where $360° < \ell < 270°$, indicating that the densest parts of Loop I extend closest to the Sun for longitudes $< 40°$.

2 Location of the heliosphere in the rim of Loop I

The Loop I regions of highest column density are located beyond ~ 100 pc, but spatially smoothed E(B-V) data show that the Loop I dust shell is apparent within 50–100 pc at high latitudes and in the first galactic quadrant (Fig. 3). The void in the dust that is centered near $\ell \sim 320°$, $b \sim -20°$ shows that the Loop I superbubble interior merges into the Local Bubble interior in the fourth galactic quadrant ($\ell = 270° - 360°$). The only interstellar cloud found near the center of the void is the G-cloud [46], where the color excess corresponding to the low observed column densities (E(B-V)< 0.001 mag) is too small for detection.

Several types of data suggest that the Sun is embedded in the rim of the evolved Loop I superbubble. The first is that the geometry of the arcs associated with Loop I places the Sun at the bubble edge. Assuming that synchrotron arcs and H° arcs associated with the North Polar Spur ($\ell \sim 10° - 30°$) form a single superbubble places the center of Loop I at $\ell = 320°$, $b = 12°$, distance 120 pc, with a radius

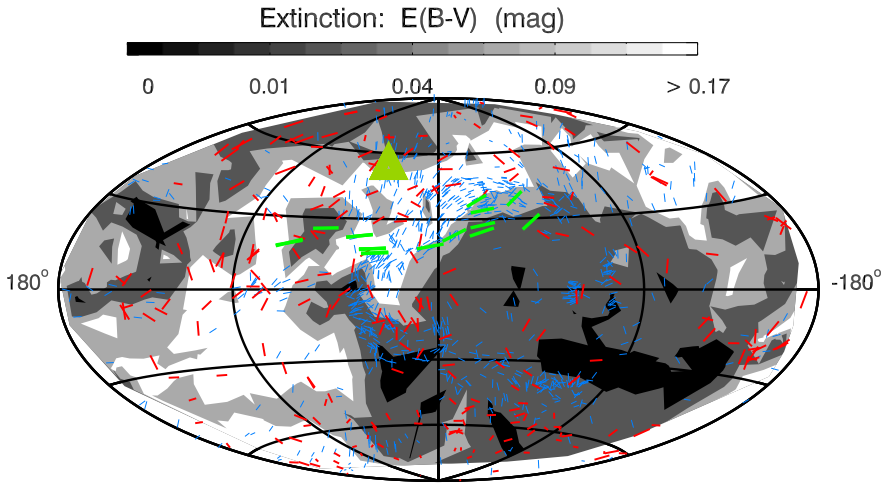

Figure 3: Smoothed contours of color excess E(B-V) for stars 50–100 pc show that dust associated with the inner rim of Loop I extends to inside of 100 pc in the North Polar Spur region. Optical polarization vectors for stars within 40 pc (red) show similar position angles in some regions when compared to more distant stellar polarizations (blue) that trace the Loop I ISMF. The filament stars are plotted in green. The green triangle identifies the IBEX Ribbon ISMF direction. The void in ISM in the fourth galactic quadrant forms where the interiors of the Loop I superbubble and Local Bubble merge. The plot is centered on $\ell = 0$, and galactic longitude increases to the left. Figure details are given in [Frisch et al., 2012].

of ~ 115 pc [5; 32]. An alternative geometric model is consistent with the series of high-latitude arcs visible in the H° data [33; 34]. The associated radio continuum arcs have been modeled as two shells by Wolleben [58], using the intensity of polarized radio continuum emission (also see [3]) and Fig. 6). The shell geometry suggests that the Sun is most likely in the rim of the shell identified as "S1" [58], which is centered at $\ell = 346° \pm 5°$, $b = 3° \pm 5°$ [14; 15; 21; 58].

The kinematical properties of nearby interstellar gas provide the second type of information suggesting that the Sun is located in the rim of Loop I. Interstellar gas within 30 pc flows past the Sun with an upwind direction in the Local Standard of Rest (LSR) that is directed toward the center of the Loop I superbubble [17; 20]. For the assumption that the different cloudlets in the flow move with a rigid body motion, the heliocentric vector flow of nearby ISM past the Sun is away from $\ell = 12.4°$, $b = 11.6°$, at a velocity of -28.1 ± 4.6 km s^{-1} [17; 20]. Using the LSR motion derived from Hipparcos data by Schonrich et al. (2010), and including the uncertainties of both the solar apex motion and the heliocentric interstellar motion, this heliocentric vector flow corresponds to the upwind LSR velocity vector of ℓ,b= $338.4° \pm 15.2°$, $-5.3° \pm 8.3°$ and 17.2 ± 4.6 km s^{-1} for the bulk CLIC motion. This is $11° \pm 19°$ from the S1 shell center. Alternate velocity vectors for local gas yield similar results. For example, a local cloud velocity derived from a restricted data set that omits outlying and redundant velocity components produced a heliocentric upwind velocity of $\ell = 5.8° \pm 0.8°$, $b = 12.8° \pm 0.7°$, velocity -25.5 ± 0.3 km s^{-1} [25], which then corresponds to the LSR velocity $\ell = 323.6° \pm 1.7°$, $b = -16.2° \pm 1.4°$

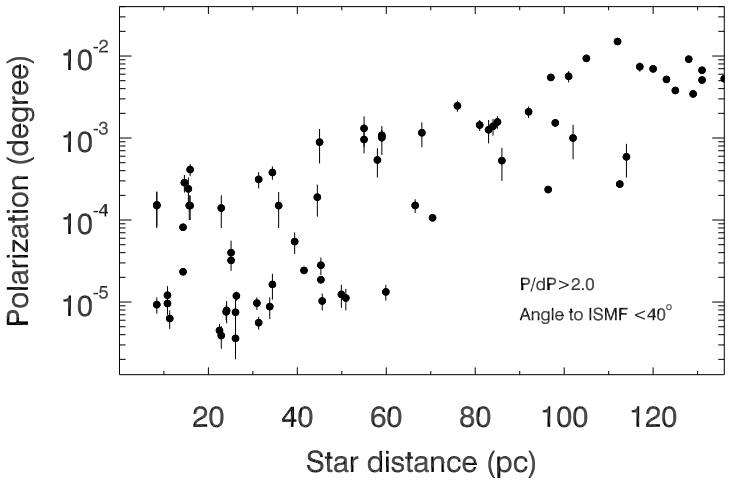

Figure 4: Polarizations are plotted against the distances of stars that are within 40° of the magnetic field direction indicated by the center of the IBEX Ribbon (see text). The steady increase in polarization with distance shows that the aligned dust grains extend to the solar location. The closest interstellar polarizations are toward stars within 5 pc, indicating that the stream of polarized dust toward Loop I must extend close to the heliosphere in the first galactic quadrant.

and a velocity of -17.0 ± 0.6 km s^{-1}. Thus, regardless of the specific assumptions about the individual components used for calculating the bulk flow, the upwind direction is always toward the low density void around the Loop I center.

The third set of data relating the CLIC with the perimeter of Loop I is plotted in Fig. 4, where the polarization strengths are shown to increase steadily with distance inside of a cone of radius 40° that is centered on the IBEX ribbon ISMF direction (also see related figures in [2] and [21). The IBEX ribbon ISMF is directed toward the North Polar Spur (Figs. 2, 3), so this polarization bridge shows that both an ISMF and a dust stream extend from the solar location out to the interstellar density jump at 100 pc in the North Polar Spur direction. The connection that we find between the ISMF direction at the heliosphere and the dominant local field direction from the polarization data [21; 22] then links the very local ISMF to the ISMF of Loop I.

This cluster of local interstellar cloudlets (CLIC) is decelerating, as shown by blue-shifted velocity components in both the upwind and downwind directions [17; 20]. Representative of this deceleration is the supersonic collision between the LIC and the BC in the direction of Sirius [15; 54].

3 Interstellar magnetic field shaping the heliosphere

The discovery of a "ribbon" of energetic neutral atoms (ENAs) by the Interstellar Boundary Explorer (IBEX) spacecraft [23; 40; 52] has provided a remarkable opportunity to understand the relation between the dominant magnetic structure in the sky, Loop I, and the ISMF that shapes the heliosphere. Optical polarization data that trace the ISMF in the low-density local interstellar medium (ISM) gives us a new

tool for probing the physical properties and history of nearby interstellar clouds. We have undertaken a project to map the local ISMF direction, and are finding that the ISMF that shapes the heliosphere is associated with the rim of the Loop I superbubble [18; 21; 22].

Although there is no generally accepted physical mechanism for the formation of the IBEX ribbon [41], most existing models indicate that it appears in sightlines that are perpendicular to the ISMF as it drapes over the heliosphere upwind of the heliopause [52]. The ribbon is extraordinarily circular, with an ellipticity of < 0.3, and is centered at galactic coordinates of $\ell = 34.7°$, $b = 56.6°$ ($\pm 2.6°$, after converting the J2000 ecliptic position in [24] to galactic coordinates). The class of models that have successfully reproduced the ribbon configuration predict that the ribbon forms ~ 50 AU upwind of the heliopause, and that the ISMF direction is within $\sim 15°$ of the center of the ribbon arc [30]. Because of the importance of interstellar pressure terms to the shape and dimensions of the outer heliosphere, the geometric configuration of the ribbon is highly sensitive to the physical properties of the surrounding interstellar cloud [19; 29; 30; 45].

The polarity of the local ISMF is not defined close to the Sun by astronomical data. It has been measured by Voyager 1 in the heliosphere depletion region, and the field was found to be directed upwards out of the ecliptic plane [6]. Observations of the Faraday rotation measures of four pulsars in the third galactic quadrant region of low interstellar densities also find that the polarity of the ISMF over ~ 100 pc scales is directed upwards through the galactic and ecliptic planes [49].

4 Structure in the local interstellar magnetic field

We have determined the magnetic field direction in the local interstellar medium where gas column densities are low, N(H^{o})$< 10^{18.7}$ cm^{-2}, dust is unreddened, E(B-V)< 0.001 mag, and interstellar optical polarizations are weak, $< 0.01\%$ [18; 21; 22]. These studies use new polarization data collected in the southern and northern hemispheres as well as data in the literature. The present analysis focuses on data for stars within 40 pc and 90° of the heliosphere nose in order to confine the study to local ISM in the upwind hemisphere of the sky.

We have developed a method [18; 21; 22] for obtaining the ISMF direction that takes advantage of the fact that a linear polarization position angle of zero degrees indicates that the starlight polarization vector is aligned with the ISMF. Testing the data sample for all possible field directions then yields the "true" field direction corresponding to the lowest value of the weighted mean of the sine of those position angles. The weighting factors allow the use of lower sensitivity polarization data. The polarization data used for this study are plotted in Fig. 3 as the red and green polarization vectors. The polarizations plotted in green consist of a distinct group of stars, here termed the "filament stars" (see below).

Frisch et al. [21] applied this analysis method to a polarization dataset and found a best-fitting magnetic field direction toward $\ell = 47° \pm 20°$, $b = 25° \pm 20°$. The angle between this ISMF direction and the IBEX ribbon field direction is $32° \pm 28°$.

In our new study [22], using an expanded dataset, we find that at least two distinct magnetic field directions are traced by the polarization data [22]. The first structure is traced by the group of stars termed here the 'filament stars'; it is well-defined both by the elongated spatial grouping (green polarizations in Fig. 3), and by the linear decrease of the polarization position angles with distance. This magnetic structure is sampled by stars as close as ~ 5 pc. More details and possible origins of this filament are given in [22].

When the filament stars are omitted from the calculations of the best-fitting ISMF, the ISMF that dominates the fit has the direction $\ell = 36°$, $b = 49°$ ($\pm 16°$). The values of the merit function for this

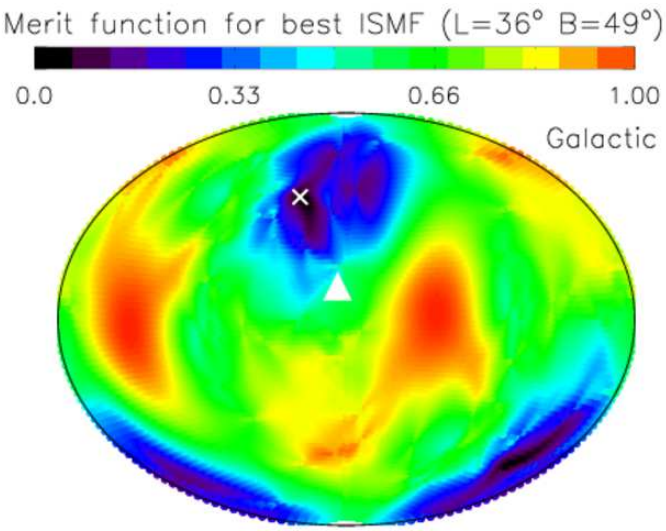

Figure 5: The spatial variations of the merit function for the best-fitting ISMF direction obtained from our polarization data set of qualifying stars (e.g.within 40 pc and 90° of the heliosphere nose) are plotted in galactic coordinates, using an Aitoff projection centered on the galactic center. The white "X" and triangle indicate the ISMF and heliosphere nose directions, respectively. The polarization data set underlying this figure omits the filament stars that trace a different magnetic field direction (see [Frisch et al., 2014] for details). The best-fitting ISMF direction is obtained by minimizing a merit function, which in essence minimizes the ensemble of polarization position angle sines. The best-fitting ISMF direction to the polarization data is within $7.6^\circ \pm 16.2^\circ$ of the magnetic field direction indicated by the IBEX ENA Ribbon [Funsten et al., 2013].

fit are plotted for magnetic field directions in all positions on the sky (Fig. 5). This ISMF direction represents the dominant magnetic structure in the hemisphere around the heliosphere nose, according to our fitting algorithm. The direction is in excellent agreement with the ISMF direction from the IBEX ribbon center to within the uncertainties. The angle between this dominant ISMF direction and the LSR velocity vector of the bulk flow of the local ISM past the Sun is $74^\circ \pm 24^\circ$. A nearly perpendicular angle between the CLIC flow velocity and the CLIC magnetic field is consistent with the expected configuration of a magnetic field that has been compressed in an expanding superbubble shell.

The strength of the ISMF can not be obtained from optical polarization data, but other data and models indicate that it is ~ 3 μG. If an ISMF strength of 3 μG is assumed in the Heerikhuisen et al. models of the ribbon [30], the ribbon center is offset from the direction of the ISMF at infinity by $\sim 4^\circ$. The offset becomes larger for weaker field strengths. Photoionization models of the Local Interstellar Cloud (LIC) around the heliosphere find a field strength of ~ 3 for equilibrium between magnetic and thermal pressures μG [55]. The pressure of the plasma in the inner heliosheath traced by IBEX ENA measurements, compared to interstellar pressures, indicates a strength for the ISMF of ~ 3.3 μG [53].

The ISMF is a conduit for TeV galactic cosmic rays that flow into the heliosphere [54]. TeV cosmic rays diffuse through the local ISM with typical gyroradii of less than 700 AU. Stellar polarization data show that the ISMF traced by the IBEX ribbon extends into the space beyond the immediate heliosphere vicinity. This supports results showing that the observed TeV cosmic ray anisotropies are consistent with cosmic ray diffusion along the ISMF traced by the IBEX ribbon [54].

The geometrical relation between the local magnetic field, the positions and kinematics of local interstellar clouds, and the Loop I S1 superbubble, suggest that the Sun is located in the boundary of this evolved superbubble. The quasi-perpendicular angle between the bulk kinematics and magnetic field of the local ISM indicates that a complete picture of low density interstellar clouds needs to include information on the interstellar magnetic field. Fig. 6 shows the projection of the Wolleben S1 shell [58] onto the galactic plane, with the bulk motion of the ISM flowing past the Sun overplotted as the thick light gray arrow, and the fifteen clouds derived in the Redfield and Linsky [46] analysis plotted as individual color-coded arrows. The S1 shell geometry is consistent with the inclusion of the CLIC within the shell.

5 What is an interstellar cloud?

Eugene Parker once asked "what is an interstellar cloud" [13]. The low density partially ionized interstellar gas in which the heliosphere is now embedded ($n(H^o) \sim 0.2$ cm^{-3}, $n(H^+) \sim 0.06$ cm^{-3}, T$\sim$ 6300 K [55]) was once identified as "intercloud medium" [48] to distinguish it from the dusty or opaque clouds that attenuate starlight. Beyond about 7 AU, the mass density of interplanetary space is dominated by neutral interstellar hydrogen. In some sense this interstellar material forms a heliospheric interstellar cloud.

Interstellar material can be characterized by volume density, column density, ionization, kinematics, turbulence, temperature, composition, and/or the magnetic field. The tradition of identifying interstellar clouds by velocity began with an early all-sky survey of interstellar absorption components toward bright stars where multiple Doppler-shifted components were resolved [1]. Since then, the Doppler-shifted velocity of a cloud has proven the easiest form of cloud identification. The shortcoming of flagging clouds by absorption line velocity is that this diagnostic depends on the instrument. Adjacent absorption components typically are blended in velocity space, and the number of identified clouds has been found to increase nearly exponentially as instrumental spectral resolution improves [13; 57]. The

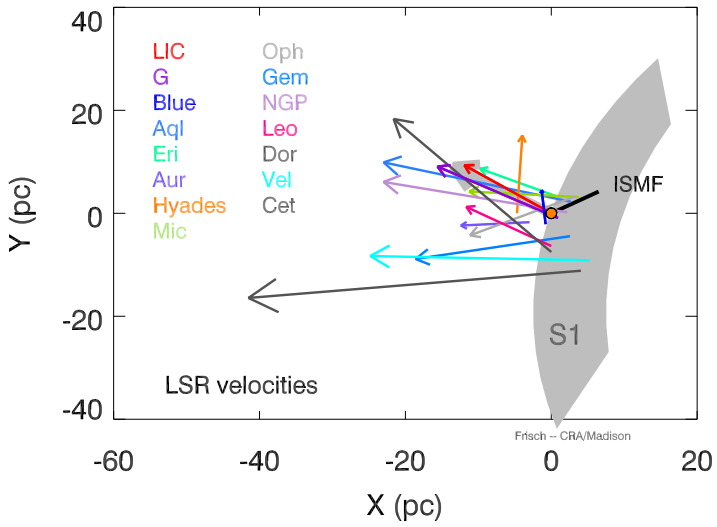

Figure 6: The Loop I S1 shell [Wolleben, 2007] and nearby cloud [Redfield and Linsky, 2008] LSR velocities [Frisch and Schwadron] are shown projected onto the galactic plane. The black line shows the ISMF direction from the IBEX ENA Ribbon center [Funsten et al., 2013]. Omitting filament stars from the calculation gives an ISMF direction from the polarization data and IBEX Ribbon that agree. The large gray arrow shows the bulk flow of local ISM through the LSR [Frisch et al., 2011]. This ISM flow is perpendicular to the the ISMF and S1 shell. The Sun is located at the orange dot.

question of "what is a cloud" then becomes even more problematical for the decelerating flow of ISM past the Sun.

This tradition of identifying clouds by velocity has been followed for the local ISM, but the concept that clouds are individual entities is transcended by the inclusion of an interstellar magnetic field. We have found that the bulk flow of local interstellar gas past the Sun has a direction that is nearly perpendicular to the direction of the local ISMF determined from optical polarization data [15; 21; 22; 54]). This connection between cloud kinematics and magnetic field extends the concept of interstellar clouds beyond velocity components, so as to include large scale structural features in the ISMF such as the Loop I superbubble. Furthermore, the ISMF shaping the heliosphere corresponds to the ISMF traced by the polarizations of nearby starlight.

A discussion of the multiple models for the "cloud-structure" of the local ISM is outside of the scope of this paper. However the comparison between the polarization data (e.g. Fig. 3]) and the 15-cloud structure modeled by Redfield and Linsky ([46], also see [20]) produces the interesting result that no significant nearby polarizations are yet found in the upwind direction toward the G-cloud. This appears to be related to the destruction of grains by interstellar shocks [22]. The relative velocities between adjacent cloud components support the presence of local shocked ISM, both between the LIC and G-cloud [16; 26], the Blue Cloud and the LIC [54], and other nearby sightlines.

6 Conclusions

Measurements of nearby interstellar gas and dust indicate that the local ISM is associated with the rim of the evolved Loop I superbubble. The bulk motion of nearby interstellar gas through the LSR indicates an upwind direction toward the center of Loop I. Both polarized starlight and the center of the IBEX ribbon indicate that the magnetic field is perpendicular to the bulk velocity of local ISM. The ISMF compressed in the rim of an expanding superbubble shell that is sweeping up interstellar material is expected to be perpendicular to the expansion velocity of the shell. The increase of polarizations with distance indicates that the source of some of the CLIC dust is part of an interstellar dust stream that connects to the nearest side of Loop I toward the North Polar Spur region.

Acknowledgements: To be published in the proceedings of the 13th Annual International Astrophysics Conference: "Voyager, IBEX, and the Interstellar Medium". This work has been partially supported by the NASA Explorer Program through funding of the IBEX project.

References

[1] W. S. Adams. Observations of interstellar H and K, molecular lines, and radial velocities in the spectra of 300 O and B stars. *ApJ*, 109:354–379, 1949.

[2] J. Bailey, P. W. Lucas, and J. H. Hough. The linear polarization of nearby bright stars measured at the parts per million level. *MNRAS*, 405:2570–2578, 2010.

[3] A. Berdyugin, V. Piirola, and P. Teerikorpi. Interstellar polarization at high galactic latitudes from distant stars. VIII. Patterns related to the local dust and gas shells from observations of ˜3600 stars. *A&A*, 561:A24, January 2014.

[4] E. M. Berkhuijsen. A survey of the continuum radiation at 820 mhz between declinations ˜7° and 850.11°. a study of the Galactic radiation and the degree of polarization with special reference to the loops and spurs. *A&A*, 14:359–386, 1971.

[5] E. M. Berkhuijsen, C. G. T. Haslam, and C. J. Salter. Are the galactic loops supernova remnants? *A&A*, 14:252–262, 1971.

[6] L. F. Burlaga, N. F. Ness, and E. C. Stone. Magnetic Field Observations as Voyager 1 Entered the Heliosheath Depletion Region. *Science*, page 1, 2013.

[7] I. A. Crawford. High resolution observations of interstellar Na I and Ca II towards the Scorpio-Centaurus association. *A&A*, 247:183–201, 1991.

[8] E. J. de Geus. Interactions of stars and interstellar matter in Scorpio Centaurus. *A&A*, 262:258–270, 1992.

[9] F. Elias, E. J. Alfaro, and J. Cabrera-Caño. Hierarchical star formation: stars and stellar clusters in the Gould Belt. *MNRAS*, 397:2–13, July 2009. doi: 10.1111/j.1365-2966.2009.14465.x.

[10] K. M. Ferriere, M.-M. Mac Low, and E. G. Zweibel. Expansion of a superbubble in a uniform magnetic field. *ApJ*, 375:239–253, 1991.

[11] P. C. Frisch. Characteristics of nearby interstellar matter. *Space Sci. Rev.*, 72:499–592, 1995.

[12] P. C. Frisch. The Galactic environment of the Sun. *American Scientist*, 88:52–59, 2000.

[13] P. C. Frisch. *The Interstellar Medium of Our Galaxy*, pages 647–676. "Kluwer Academic Publishers", 2001.

[14] P. C. Frisch. The S1 Shell and Interstellar Magnetic Field and Gas Near the Heliosphere. *ApJ*, 714:1679–1688, 2010.

[15] P. C. Frisch and N. A. Schwadron. Large-scale Interstellar Structure and the Heliosphere.

[16] P. C. Frisch and D. G. York. The distribution of nearby HI and H II gas. In R. F. Malina and S. C. Bowyer, editors, *Extreme Ultraviolet Astronomy*, page 322, Tarrytown, NY, 1991. Pergamon.

[17] P. C. Frisch, L. Grodnicki, and D. E. Welty. The Velocity Distribution of the Nearest Interstellar Gas. *ApJ*, 574:834–846, 2002.

[18] P. C. Frisch, B. Andersson, A. Berdyugin, H. O. Funsten, M. Magalhaes, D. J. McComas, V. Piirola, N. A. Schwadron, J. D. Slavin, and S. J. Wiktorowicz. Comparisons of the Interstellar Magnetic Field Directions obtained from the IBEX Ribbon and Interstellar Polarizations. *ApJ*, 724:1473–1479, 2010a.

[19] P. C. Frisch, J. Heerikhuisen, N. V. Pogorelov, B. DeMajistre, G. B. Crew, H. O. Funsten, P. Janzen, D. J. McComas, E. Moebius, H.-R. Mueller, D. B. Reisenfeld, N. A. Schwadron, J. D. Slavin, and G. P. Zank. Can IBEX Identify Variations in the Galactic Environment of the Sun Using Energetic Neutral Atoms? *ApJ*, 719:1984–1992, 2010b.

[20] P. C. Frisch, S. Redfield, and J. Slavin. The Interstellar Medium Surrounding the Sun. *ARA&A*, 49, 2011.

[21] P. C. Frisch, B.-G. Andersson, A. Berdyugin, V. Piirola, R. DeMajistre, H. O. Funsten, A. M. Magalhaes, D. B. Seriacopi, D. J. McComas, N. A. Schwadron, J. D. Slavin, and S. J. Wiktorowicz. The Interstellar Magnetic Field Close to the Sun. II. *ApJ*, 760:106, 2012.

[22] P. C. Frisch, B.-G. Andersson, A. Berdyugin, V. Piirola, H. O. Funsten, A. M. Magalhaes, D. B. Seriacopi, D. J. McComas, N. A. Schwadron, J. D. Slavin, and S. J. Wiktorowicz. Structure in the Local Interstellar Magnetic Field: Identifying the component that extends to the heliosphere location. *ApJ, in preparation*, 2014.

[23] H. O. Funsten, F. Allegrini, G. B. Crew, R. DeMajistre, P. C. Frisch, S. A. Fuselier, M. Gruntman, P. Janzen, D. J. McComas, E. Möbius, B. Randol, D. B. Reisenfeld, E. C. Roelof, and N. A. Schwadron. Structures and Spectral Variations of the Outer Heliosphere in IBEX Energetic Neutral Atom Maps. *Science*, 326:964–967, 2009.

[24] H. O. Funsten, R. DeMajistre, P. C. Frisch, J. Heerikhuijsen, D .M. Higdon, P. Janzen, B. Larsen, G. Livadiotis, D. J. McComas, E. Möbius, C. Reese, D. B. Reisenfeld, N. A. Schwadron, and E. J. Zirnstein. Circularity of the IBEX Ribbon of Enhanced Energetic Neutral Atom (ENA) Fluxes. *ApJ*, 776:30, 2013.

[25] C. Gry and E. B. Jenkins. The interstellar cloud surrounding the Sun – a new perspective. *ArXiv e-prints*, 2014.

[26] S. Grzedzielski and R. Lallement. Possible Shock Wave in the Local Interstellar Plasma, Very Close to the Heliosphere. *Space Sci. Rev.*, 78:247–258, 1996.

[27] J. Han. The magnetic structure of our Galaxy: a review of observations. *IAU Symposium*, 259: 455–466, 2009.

[28] D. Hartmann and W. Burton. *Atlas of Galactic Neutral Hydrogen*. 2012.

[29] J. Heerikhuisen and N. V. Pogorelov. An Estimate of the Nearby Interstellar Magnetic Field Using Neutral Atoms. *ApJ*, 738:29–+, 2011.

[30] J. Heerikhuisen, E. J. Zirnstein, H. O. Funsten, N. V. Pogorelov, and G. P. Zank. The Effect of New Interstellar Medium Parameters on the Heliosphere and Energetic Neutral Atoms from the Interstellar Boundary. *ApJ*, 784:73, 2014.

[31] C. Heiles. A comprehensive view of the Galactic magnetic field, especially near the Sun. In *ASP Conf. Ser. 97: Polarimetry of the Interstellar Medium*, page 457, 1996.

[32] C. Heiles. The Magnetic Field Near the Local Bubble. In D. Breitschwerdt, M. J. Freyberg, and J. Truemper, editors, *IAU Colloq. 166: The Local Bubble and Beyond*, volume 506 of *Lecture Notes in Physics, Berlin Springer Verlag*, pages 229–238, 1998a.

[33] C. Heiles. Whence the Local Bubble, Gum, Orion? GSH 238+00+09, A nearby major superbubble toward Galactic longitude 238 degrees. *ApJ*, 498:689–703, 1998b.

[34] C. Heiles, Y. . Chu, T. H. Troland, R. J. Reynolds, and I. Yegingil. A new look at the North Polar Spur. *ApJ*, 242:533–540, 1980.

[35] D. . C. Iwan. X-ray observations of the north polar spur. *ApJ*, 239:316–327, 1980.

[36] A. Lazarian. Tracing magnetic fields with aligned grains. *J. Quant. Spec. Radiat. Transf.*, 106: 225–256, July 2007.

[37] M. MacLow and R. McCray. Superbubbles in disk galaxies. *ApJ*, 324:776–785, 1988.

[38] J. Maíz-Apellániz. The Origin of the Local Bubble. *ApJ*, 560:L83–L86, 2001.

[39] D. S. Mathewson and V. L. Ford. Polarization observations of 1800 stars. *MmRAS*, 74:139–182, 1970.

[40] D. J. McComas, F. Allegrini, P. Bochsler, M. Bzowski, E. R. Christian, G. B. Crew, R. DeMajistre, H. Fahr, H. Fichtner, P. C. Frisch, H. O. Funsten, S. A. Fuselier, G. Gloeckler, M. Gruntman, J. Heerikhuisen, V. Izmodenov, P. Janzen, P. Knappenberger, S. Krimigis, H. Kucharek, M. Lee, G. Livadiotis, S. Livi, R. J. MacDowall, D. Mitchell, E. Möbius, T. Moore, N. V. Pogorelov, D. Reisenfeld, E. Roelof, L. Saul, N. A. Schwadron, P. W. Valek, R. Vanderspek, P. Wurz, and G. P. Zank. Global Observations of the Interstellar Interaction from the Interstellar Boundary Explorer (IBEX). *Science*, 326:959–, 2009.

[41] D. J. McComas, W. S. Lewis, and N. A. Schwadron. IBEXs Enigmatic Ribbon in the sky and its many possible sources. *Reviews of Geophysics*, 2014.

[42] Planck Collaboration. Planck intermediate results. XXI. Comparison of polarized thermal emission from Galactic dust at 353 GHz with optical interstellar polarization. *ArXiv e-prints*, 2014.

[43] Planck Collaboration Planck intermediate results. XIX. An overview of the polarized thermal emission from Galactic dust. *ArXiv e-prints*, May 2014.

[44] R. J. Rand and S. R. Kulkarni. The local Galactic magnetic field. *ApJ*, 343:760–772, 1989.

[45] R. Ratkiewicz, M. Strumik, and J. Grygorczuk. The Effects of Local Interstellar Magnetic Field on Energetic Neutral Atom Sky Maps. *ApJ*, 756:3, 2012.

[46] S. Redfield and J. L. Linsky. The Structure of Local Interstellar Medium. IV. *ApJ*, 673:283–314, 2008.

[47] W. Reis and W. J. B. Corradi. Mapping the interface between the Local and Loop I bubbles using Strömgren photometry. *A&A*, 486:471–484, August 2008.

[48] J. B. Rogerson, D. G. York, J. F. Drake, E. B. Jenkins, D. C. Morton, and L. Spitzer. Spectrophotometric results from the Copernicus satellite. III. Ionization and composition of the intercloud medium. *ApJ*, 181:L110–L114, 1973.

[49] M. Salvati. The local Galactic magnetic field in the direction of Geminga. *A&A*, 513:A28+, April 2010.

[50] F. P. Santos, W. Corradi, and W. Reis. Optical Polarization Mapping toward the interface between the Local Cavity and Loop I. *ApJ*, 728:104, 2011.

[51] R. Schonrich, J. Binney, and W. Dehnen. Local kinematics and the local standard of rest. *MNRAS*, 403:1829–1833, 2010.

[52] N. A. Schwadron, M. Bzowski, G. B. Crew, M. Gruntman, H. Fahr, H. Fichtner, P. C. Frisch, H. O. Funsten, S. Fuselier, J. Heerikhuisen, V. Izmodenov, H. Kucharek, M. Lee, G. Livadiotis, D. J. McComas, E. Moebius, T. Moore, J. Mukherjee, N. V. Pogorelov, C. Prested, D. Reisenfeld, E. Roelof, and G. P. Zank. Comparison of Interstellar Boundary Explorer Observations with 3D Global Heliospheric Models. *Science*, 326:966–, 2009.

[53] N. A. Schwadron, F. Allegrini, M. Bzowski, E. R. Christian, G. B. Crew, M. Dayeh, R. DeMajistre, P. Frisch, H. O. Funsten, S. A. Fuselier, K. Goodrich, M. Gruntman, P. Janzen, H. Kucharek, G. Livadiotis, D. J. McComas, E. Moebius, C. Prested, D. Reisenfeld, M. Reno, E. Roelof, J. Siegel, and R. Vanderspek. Separation of the Interstellar Boundary Explorer Ribbon from Globally Distributed Energetic Neutral Atom Flux. *ApJ*, 731:56–77, 2011.

[54] N. A. Schwadron, F. C. Adams, E. R. Christian, P. Desiati, P. Frisch, H. O. Funsten, J. R. Jokipii, D. J. McComas, E. Moebius, and G. P. Zank. Global Anisotropies in TeV Cosmic Rays Related to the Suns Local Galactic Environment from IBEX. *Science*, 343:988–990, 2014.

[55] J. D. Slavin and P. C. Frisch. The boundary conditions of the heliosphere: photoionization models constrained by interstellar and in situ data. *A&A*, 491:53–68, 2008.

[56] J. P. Vallee. Effects of interstellar magnetic bubbles and of galactic tides on galactic magnetic fields. *A&A*, 136:373–377, 1984.

[57] D. E. Welty and L. M. Hobbs. A high-resolution survey of interstellar K I absorption. *ApJS*, 133: 345–393, 2001.

[58] M. Wolleben. A New Model for the Loop I (North Polar Spur) Region. *ApJ*, 664:349–356, July 2007.